

Coronal Implosion and Particle Acceleration in the Wake of a Filament Eruption

Rui Liu & Haimin Wang

Space Weather Research Laboratory, Center for Solar-Terrestrial Research, NJIT, Newark, NJ 07102; rui.liu@njit.edu

ABSTRACT

We study the evolution of a group of *TRACE* 195 Å coronal loops overlying a reverse S-shaped filament on 2001 June 15. These loops were initially pushed upward with the filament ascending and kinking slowly, but as soon as the filament rose explosively, they began to contract at a speed of $\sim 100 \text{ km s}^{-1}$, and sustained for at least 12 min, presumably due to the reduced magnetic pressure underneath with the filament escaping. Despite the contraction following the expansion, the loops of interest remained largely intact during the filament eruption, rather than formed via reconnection. These contracting loops naturally formed a shrinking trap, in which hot electrons of several keV, in an order of magnitude estimation, can be accelerated to nonthermal energies. A single hard X-ray burst, with no corresponding rise in *GOES* soft X-ray flux, was recorded by the Hard X-ray Telescope (HXT) on board *Yohkoh*, when the contracting loops expectedly approached the post-flare arcade originating from the filament eruption. HXT images reveal a coronal source distinctly above the top of the soft X-ray arcade by $\sim 15''$. The injecting electron population for the coronal source (thin target) is hardening by ~ 1.5 powers relative to the footpoint emission (thick target), which is consistent with electron trapping in the weak diffusion limit. Although we can not rule out additional reconnection, observational evidences suggest that the shrinking coronal trap may play a significant role in the observed nonthermal hard X-ray emission during the flare decay phase.

Subject headings: Sun: flares—Sun: X-rays, gamma rays—Sun: filaments

1. Introduction

In the standard flare model (CSHKP model; Carmichael 1964; Sturrock 1966; Hirayama 1974; Kopp & Pneuman 1976), the initial driver of the flare process is a rising filament above the polarity inversion line. The rising filament stretches the overlying field lines, resulting in the formation of a current sheet underneath and the consequent cancelation of magnetic fluxes of opposite polarity. It is energetically impossible, however, to open up the closed magnetic field lines via a purely ideal-MHD process in the force-free configuration (the Aly-Sturrock paradox; Aly 1984; Sturrock

1991). One way to avoid this constraint is to open only a portion of the closed field lines (see the review by Lin et al. 2003). Considering a flux rope confined by an overlying magnetic arcade, Sturrock et al. (2001) demonstrated that it is energetically favorable for part of the rope to erupt into interplanetary space.

This *partial eruption* concept has been further investigated both observationally (e.g., Gilbert et al. 2000, 2001, 2007; Liu et al. 2007, 2008a; Tripathi et al. 2009) and numerically (e.g., Manchester et al. 2004; Fan 2005; Gibson & Fan 2006; Birn et al. 2006; Fan & Gibson 2007), especially in the context of eruptions driven by the kink instability. In particular, Fan (2005) demonstrated that the evolution of the kink instability facilitates the loss of confinement of a flux rope. Specifically, the writhing rotation changes the direction of the rope apex relative to the overlying arcade, which helps the flux rope to “rupture” through the arcade field. Gibson & Fan (2006) extended Fan’s simulation in time to show that the flux rope bifurcates into two, with one part erupting and the other staying behind. In the latter simulation, one can see that overlying loops are pushed upward and aside as the flux rope kinks and expands, and that following the rupture of the arcade, those overlying loops that have not reconnected with the rope field quickly contract back to the core field, which is reasonable, considering the reduction of the magnetic pressure in the core field due to the rope escaping. This is reminiscent of the “implosion” conjecture proposed by Hudson (2000), to which Liu et al. (2009a) lent support in observation. In that case, however, the reduction of the magnetic pressure is presumably due to the release of the free magnetic energy during the early phase of the flare.

In this Letter, we present observations of the coronal loop contraction in the wake of a filament eruption. The eruption occurred in the active region NOAA 9502 (S27E43) on 2001 June 15, associated with a *GOES* class M6 flare starting at about 10:00 UT. By studying the photospheric helicity transportation, Romano et al. (2005) concluded that the reverse S-shaped filament erupted due to the accumulation of magnetic helicity exceeding the kink instability threshold. Here we concentrate on a late-phase hard X-ray (HXR) burst recorded by *Yohkoh* (see the *Yohkoh* flare catalogue*), which occurred about 26 minutes later in the same active region, following the loop contraction. We will analyze the observations in Section 2, discuss the results in Section 3, and make concluding remarks in Section 4.

2. Observation and Analysis

2.1. Coronal Implosion

The reverse S-shaped filament is obviously visible in Figure 1(a) as a dark, absorption structure in the bright active region, as observed with the *TRACE* 195 Å filter. A bundle of brightening

*<http://gedas22.stelab.nagoya-u.ac.jp/HXT/catalogue/index.html>; HXT event number: 26710

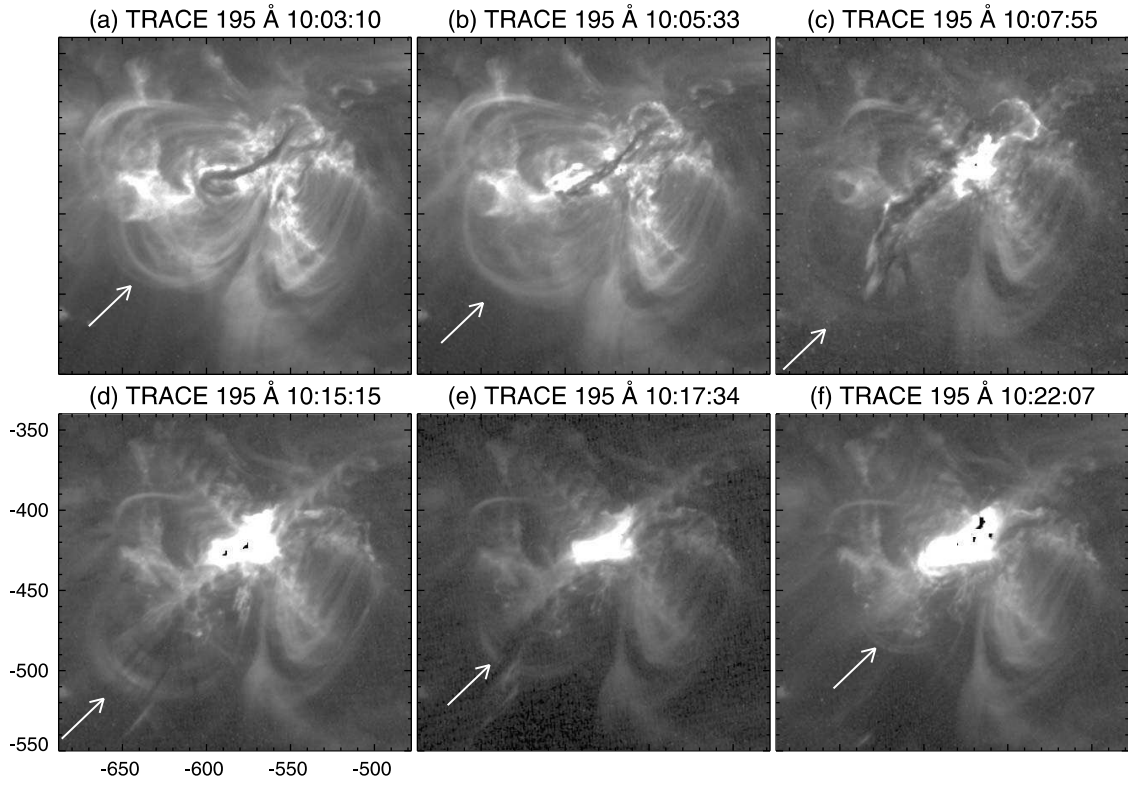


Fig. 1.— Snapshots of the expansion and contraction of coronal loops associated with a filament eruption. Images are observed with the *TRACE* 195 Å filter. The loops of interest are marked by white arrows.

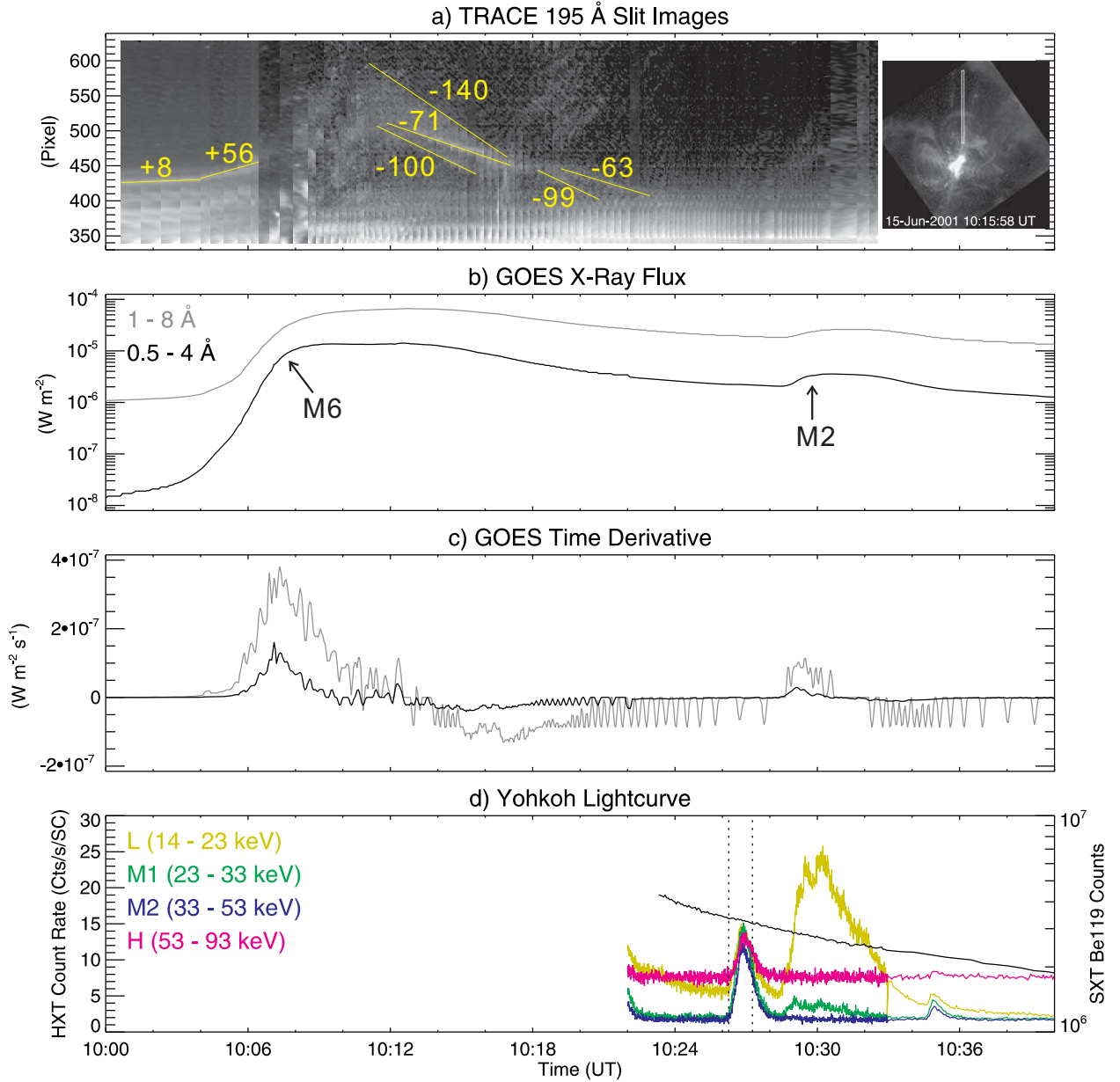


Fig. 2.— Coronal implosion observed in EUV and the lightcurves of the associated flare. (a) Slices of *TRACE* 195 Å images cut by the slit as shown in the inset are placed on the time axis. The *TRACE* image in the inset has been rotated clockwise for 145°. Labels indicate speeds derived from the apparent “slopes”, in km s^{-1} . (b) *GOES* soft X-ray fluxes in 1–8 Å (grey) and 0.5–4 Å (dark). (c) Time derivatives of *GOES* fluxes. (d) HXT counts per second and per subcollimator (SC) are scaled by the y-axis on the left, and SXR counts recorded by the Soft X-ray Telescope (SXT) Be-119 filter (integrating over the post-flare arcade of the M6 flare) are scaled by the y-axis on the right. Dotted lines mark the time interval for the HXT image synthesis.

loops astride the filament are marked by an arrow. The loops are supposed to connect the opposite polarity separated by the filament channel (c.f. §2.2). From about 09:57 UT to 10:06 UT, as the filament ascended slowly with a counterclockwise rotation of its axis (also see Green et al. 2007), the overlying loops are observed to rise with it (Figure 1(a–c)), presumably being pushed upward by the filament, but to contract (Figure 1(d–f)) from 10:11 UT onward, after the filament “broke” through the arcade at about 10:08 UT (Figure 1(c)); a comprehensive animation of *TRACE* images for this event is available at the *TRACE* website[†]. Lightcurves of the flare associated with the filament eruption are presented in Figure 2. Within one hour of the eruption, one can see that the filament channel in $H\alpha$ was filled with dark material again (Figure 3(d)), and that post-flare loops are shown as dark features perpendicular to the channel, suggestive of the partial eruption nature of the event.

To study the loop evolution in detail, we rotate *TRACE* images clockwise by 145° so that the loops of interest are positioned upward (see the inset of Figure 2(a)). A slit of 290 pixels long and 10 pixels wide is placed across the group of coronal loops, and the slices of *TRACE* images cut by the slit are placed on the time axis in Figure 2(a). Initially, the loops expanded slowly at about 8 km s^{-1} , and then at a faster speed of about 56 km s^{-1} , roughly the same speed of the rising filament. At about 10:06 UT, the filament started to rise upward explosively, simultaneously with the onset of the flare impulsive phase, as indicated by the time derivatives of *GOES* soft X-ray (SXR) fluxes (Figure 2c), which usually resemble the HXR profile (Neupert effect; Neupert 1968). At 10:07:55 UT (Figure 1(c)), the filament already lost its coherent shape, and the slit was filled by dark filament material during 10:06–10:08 UT (Figure 2(a)). The group of loops became very diffuse and faint due to shorter exposures with enhanced brightening in the flaring region. But one can still see that as early as about 10:11 UT, the loops began to contract inward at various speeds ranging from 60 km s^{-1} to 140 km s^{-1} . As an instructive comparison, the contraction of coronal loops observed in the flare early phase is at $\sim 5 \text{ km s}^{-1}$ (Liu et al. 2009a), while the shrinkage speed of relaxing cusp-shaped field lines observed in SXRs is only $\sim 2 \text{ km s}^{-1}$ (Lin 2004, and references therein).

The contraction is observed to sustain for at least 12 minutes from 10:11 to 10:23 UT. During that period the loops of interest contracted from the maximum projected height of $\sim 1.3 \times 10^{10} \text{ cm}$, with respect to the flare footpoints (see Figure 3(e)), to a height of $\sim 6 \times 10^9 \text{ cm}$, where they became hardly visible, being overwhelmed by the bright active region. The post-flare arcade originating from the M6 flare is about $4 \times 10^9 \text{ cm}$ high (projected). At an average speed of 100 km s^{-1} , the contracting loops are expected to be stopped above the arcade in $\geq 200 \text{ s}$, i.e., at about 10:26 UT, coincident with the HXR burst.

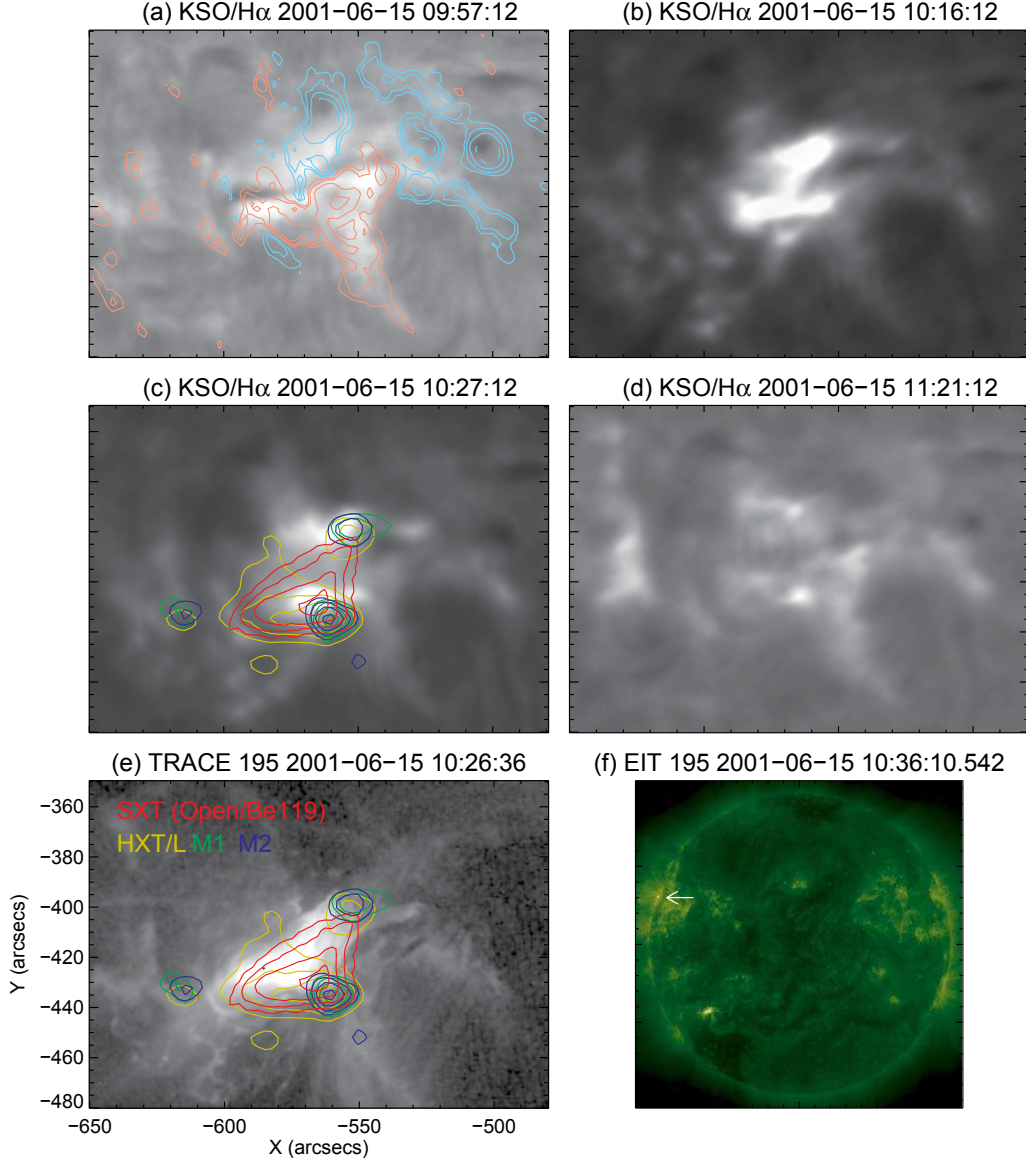


Fig. 3.— Multi-wavelength observations of the M6 flare and the late-phase HXR burst. (a) A pre-flare H α image taken by the the Kanzelhöhe Solar Observatory (KSO) is overlaid with an line-of-sight magnetogram obtained by the Michelson Doppler Imager (MDI) on board *SOHO* at 09:35 UT. Contours levels are 100, 200, 400 and 800 G for positive polarities (reddish orange), and -800, -400, -200, and -100 G for negative polarities (sky blue) (b) A H α image shows the classical two-ribbon flare associated with the filament eruption. (c) HXT and SXT contours for the late-phase burst are overlaid on the KSO H α image taken at approximately the same time. The contour levels are 10, 20, 40 and 80% of the maximum brightness. (d) shows a post-flare H α image. (e) The same contours as in (c) are overlaid on a *TRACE* 195 Å image taken at approximately the same time. The field of view is the same for panels (a)–(e). (f) shows a full-disk *SOHO* EIT 195 Å image taken at 10:36 UT. A brightening at the east limb is marked by an arrow.

Table 1. Spectral Characteristics of the late-phase HXR burst

Algorithm	γ^{CS}		γ^{SFP}		γ^{NFP}		T^{CS} (MK)	
	L/M1	M1/M2	L/M1	M1/M2	L/M1	M1/M2	L/M1	M1/M2
MEM	...	3.7 ± 1.1	1.6 ± 0.4	3.2 ± 0.3	...	3.1 ± 0.6	...	163 ± 64
Pixon	...	3.1 ± 0.7	1.8 ± 0.3	2.6 ± 0.2	...	2.3 ± 0.3	...	218 ± 94

Note. — Spectral information from HXT images is derived by calculating flux ratios between adjacent energy bands. A region growing method is used to specify the integration region for each individual HXR source (see Liu et al. 2009b, for details). CS stands for coronal source. SFP (NFP) is referred to the footpoint source located in the south (north).

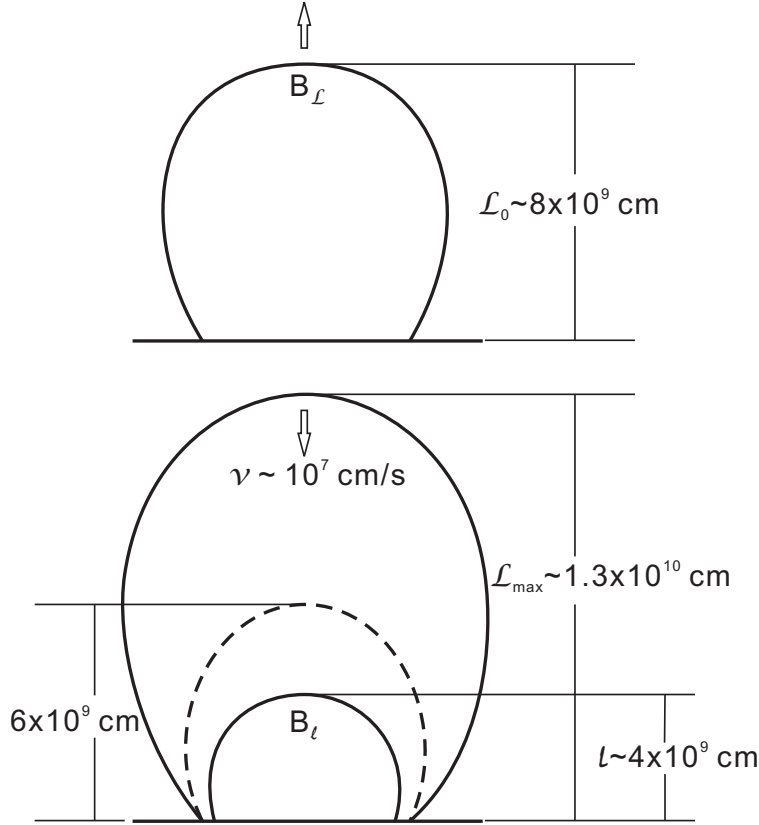


Fig. 4.— Cartoon of a shrinking trap as a simplification of the observations. Top panel shows that initially the loop is pushed upward. Bottom panel shows that the loop shrinks toward the post-flare arcade. L_0 is the loop's initial height ($\sim 8 \times 10^9 \text{ cm}$) measured from *TRACE* images. Similarly, L_{max} is the loop's maximum height ($\sim 1.3 \times 10^{10} \text{ cm}$), and l the height of the post-flare arcade ($\sim 4 \times 10^9 \text{ cm}$). v is the average contraction speed. B_l and B_L denote the magnetic field at the height of l and L_0 , respectively. The dotted line indicates the loop position at 10:23 UT.

2.2. Above-The-Loop-Top Hard X-Ray Source

The HXR burst observed by *Yohkoh* HXT features a single peak that lasts for about 2 min. The four HXT bands show a similar profile (Figure 2(d)), with no corresponding rise in SXR (Figure 2(b) and (c)). The dotted lines in Figure 2(d) mark the time interval of data accumulation for reconstructing HXR sources. The images synthesized with the Maximum Entropy Method (MEM) are shown as contours in Figure 3 (c) and (e), which are very similar to those reconstructed with the Pixon method (therefore are not shown here). Note three minutes later ($\sim 10:29$ UT), an M2 flare was recorded by *GOES*, which, however, is pinpointed to a different active region (NOAA 9506), in view of the following observations: 1) The *SOHO* EIT 195 Å image taken at 10:36 UT (Figure 3(f)) shows a brightening point at the east limb (marked by an arrow), with no corresponding brightening in the previous EIT image at 10:24 UT (not shown); 2) HXT L- and M1-band images (not shown) synthesized during the M2 flare also exhibit a point source co-spatial with the 195 Å brightening; 3) The SXR counts integrating over the post-flare arcade of the M6 flare decrease exponentially during the M2 flare (Figure 2(d)).

The most striking feature of HXR burst is the existence of a coronal HXR source whose centroid position is about $15''$ above the SXT loop top (Figure 3(e)). No significant SXR emission was detected at the coronal source location, indicating a rather low thermal plasma density. In addition, the coronal source is so lacking in L-band emission that no plausible spectral index can be derived from the L and M1 channel ratio (Table 1). In fact, the whole HXR burst is also relatively lacking in L-band photons (see Figure 2(d)). This indicates a short of low-energy electrons, which normally would have constitute the bulk of the total energy. Thus, the energy input into the chromosphere may be too small to drive chromospheric evaporation, which explains the absence of the Neupert effect (Veronig et al. 2005; Warmuth et al. 2009).

On the other hand, the spectral index of the coronal emission derived from the M1 and M2 channel ratio is rather hard, similar to those of the footpoints (Table 1). As a result, thermal interpretation cannot yield plausible temperatures. One may wonder whether the presumed coronal source is actually a third footpoint. However, this is not supported by the bipolar magnetic configuration involved in this classical two-ribbon flare (Figure 3(a)–(c)), nor by the apparent bipolar coronal loops in the active region (Figure 1). Moreover, one can see in Figure 3(c) that the conjugate footpoints are located at the two flare ribbons, while no visible $H\alpha$ brightening is observed at the coronal source location.

If we assume the thin-target hypothesis for the coronal source ($\delta^{\text{CS}} = \gamma_2^{\text{CS}} - 1^\dagger$), and thick-target for the footpoint emission ($\delta^{\text{FP}} = \gamma_2^{\text{FP}} + 1$), then the injecting electron population for

[†]http://trace.lmsal.com/POD/bigmovies/filaments/T195_2001Jun15New.mov

[‡]We denote the photon spectral index derived from the L- and M1-band ratio as γ_1 , and that from the M1- and M2-band as γ_2 , with the superscripts, CS and FP, standing for the coronal source and the footpoint, respectively. Corresponding electron power-law indices are denoted by δ in a usual fashion.

the coronal source, δ^{CS} , is hardening by about 1.5 powers, relative to that for the footpoint, δ^{FP} , which is consistent with electron trapping in the weak diffusion limit (c.f., the Appendix in Metcalf & Alexander 1999).

3. Discussion

The characteristics of the above-the-loop-top source presented in this Letter are reminiscent of the famous Masuda flare (Masuda et al. 1994), which is regarded as a very unique event (see the review by Krucker et al. 2008). In a recent revisit of the Masuda flare (Liu et al. 2009b), however, we noticed that in the calibrated HXT images (Sato et al. 1999), the coronal source looks like a normal *loop-top* source, located slightly above the SXT loop top but within the 10% brightness contour of the HXT L-band thermal loop, rather than *distinctly above the loop top* as in the original HXT images (e.g., Figure 3 in Aschwanden et al. 1996). Accordingly, its spectral indices also fall into the normal range of coronal emission (4–7; Tomczak 2001; Krucker & Lin 2008). These changes have relieved, in large measure, the longstanding difficulties of understanding the original Masuda flare, viz., the lack of L-band emission of the coronal source, and the low density at the coronal source location.

On the other hand, the so called above-the-loop-top sources reported in the *RHESSI* era have been primarily, if not exclusively, found in a double coronal source morphology (Sui & Holman 2003; Sui et al. 2004; Pick et al. 2005; Veronig et al. 2006; Li & Gan 2007; Liu et al. 2008b). In that case, the lower coronal source is located at the thermal loop top, while the upper source can be located as far as $30''$ above the lower one, moving upward at a speed as high as 300 km s^{-1} (e.g., Sui & Holman 2003). The two sources “mirror” each other with respect to a presumed X-point reconnection site, in that higher energy emission comes from lower altitudes for the upper source, while the lower source exhibits a reversed order (e.g., Sui & Holman 2003; Liu et al. 2008b). The spectra of the two sources have a similar power-law index (Liu et al. 2008b), suggesting that the injecting populations are intimately related, presumably accelerated at the X-point. If an X-point configuration were assumed below the above-the-loop-top source studied here, as illustrated in Figure 3(c), an additional loop-top source should also be expected, which is obviously not the case.

Alternatively, the contracting loops may be relevant in the HXR production, since a shortening of the field line length indicates a reduction of the magnetic energy intensity, which is available as free energy to heat and accelerate particles. This effect has been discussed in the context of newly reconnected cusp-shaped lines relaxing into potential-like lines at lower altitudes (Somov & Kosugi 1997).

As a simplification of our observation, Figure 4 illustrates that a magnetic loop is initially stretched and pushed upward (top panel), and later forms a shrinking trap (bottom panel) in which mirroring particles are accelerated in a way similar to the trap-without-shock scenario in

Somov & Kosugi (1997). The lifetime of our shrinking trap,

$$T \simeq \frac{L_{max} - l}{v} \simeq \frac{9 \times 10^9 \text{ cm}}{10^7 \text{ cm s}^{-1}} = 900 \text{ s},$$

where v , the shrinking speed of the coronal loop, is approximated to be 100 km s^{-1} (see Figure 2(a)). The collisional deflection time of an electron of energy E is given by,

$$t(E) = 0.95 \left(\frac{E}{1 \text{ keV}} \right)^{3/2} \left(\frac{n_e}{10^8 \text{ cm}^{-3}} \right)^{-1} \left(\frac{20}{\ln \Lambda} \right) \text{ s},$$

where the Coulomb logarithm, $\ln \Lambda = \ln(8 \times 10^6 T_e n_e^{-1/2}) \simeq 20$ under typical coronal conditions. Thus, for 10–100 keV electrons in the coronal trap with a density in the order of 10^8 cm^{-3} , the trapping time is of order 100–1000 s, comparable to the trap lifetime.

For an 1–10 keV electron, its thermal speed $v_e \simeq (2 - 6) \times 10^9 \text{ cm s}^{-1}$, so its characteristic time between two subsequent reflections, $\tau \leq 2L_{max}/v_e \simeq (4 - 13) \text{ s}$. Since $\tau \ll T$, the conditions of the periodic longitudinal motions change adiabatically. The longitudinal adiabatic invariant is therefore conserved (Somov 2006, Chapter 6), i.e.,

$$P_{\parallel}(t) L(t) = \text{const.}$$

Since $L_{max}/l \simeq 3.3$, when $t \rightarrow T$, $P_{\parallel}(t) \rightarrow 3.3 P_{\parallel}(0)$. In addition, the transversal adiabatic invariant is conserved in the non-relativistic approximation,

$$\frac{P_{\perp}^2(t)}{B} = \text{const.}$$

Assuming that both the initial and the final state of the magnetic loop are quasi-potential, we estimate the field strength at the loop top, following the empirical formula from Dulk & McLean (1978), i.e.,

$$B_l \simeq 0.5 (l/R_{\odot})^{-3/2} \simeq 36 \text{ G},$$

and $B_L \simeq 0.5 (L_0/R_{\odot})^{-3/2} \simeq 13 \text{ G}$, where B_l and B_L denote the magnetic field at the height of l and L_0 , respectively. As the contracting loop approaches the post-flare arcade (bottom panel of Figure 4), $B \rightarrow B_l$, hence $P_{\perp}(t) \rightarrow 1.7 P_{\perp}(0)$, and $E_k(t) = (P_{\perp}(t)^2 + P_{\parallel}(t)^2)/2m_e \rightarrow 14 E_k(0)$. Thus, hot electrons of several keV can be accelerated to nonthermal energies in this trap.

4. Conclusion

We suggest that the escaping of the kinking filament in the 2001 June 15 event results in the contraction of the overlying coronal loops, which can be regarded as a variant of coronal implosion (Hudson 2000; Liu et al. 2009a). The contracting loops form a natural shrinking trap, which can efficiently accelerate electrons. This explains the HXR burst during the flare decay phase, which

is characterized by nonthermal coronal emission in consistency with electron trapping in the weak diffusion limit. Although magnetic reconnection cannot be excluded in this picture, the shrinking trap model seems to offer a more self-consistent interpretation.

We expect this acceleration process to occur generally in eruptions in which the arcade field is only partially opened. Free energy builds up in the arcade when field lines are pushed upward by the eruptive flux rope, since the magnetic energy associated with the loop,

$$W = \frac{1}{8\pi} \int \int B^2 ds dl,$$

where s is the loop cross section, assuming to be constant, and l the loop length. As the stretched field relaxes in the wake of the rope escaping, trapped particles gain energy from the increase in parallel momentum, due to shortening field lines, and from the increase in perpendicular momentum, due to strengthening magnetic field at lower altitudes.

This process may play a role in some of the HXR bursts observed during the flare late phase, which often show weak soft emission, hardening spectra, and/or high coronal sources (e.g., Frost & Dennis 1971; Hudson 1978; Grigis & Benz 2008; Warmuth et al. 2009). Such late-phase bursts have been often attributed to the acceleration and trapping of electrons in the post-flare loop systems (e.g., Cliver et al. 1986), or, to the acceleration of electrons in a shock front (e.g., Frost & Dennis 1971). The mechanism suggested here, however, involves a transfer of the free magnetic energy from the core field to the confining arcade during the eruptive process. The energy transferred is then made available to the trapped particles in the aftermath of the partial eruption, through the contraction of the loops that have not reconnected.

The authors thank the anonymous referee for helpful comments. We would like to acknowledge the *TRACE* and *Yohkoh* consortia for the excellent data. RL thanks J. Lin for helpful discussion, and Y. Xu for processing KSO H α data, which are provided through the Global High Resolution H-alpha Network. This work was supported by NASA grant NNX08-AJ23G and NNX08-AQ90G, and by NSF grant ATM-0849453.

REFERENCES

- Aly, J. J. 1984, *ApJ*, 283, 349
- Aschwanden, M. J., Hudson, H., Kosugi, T., & Schwartz, R. A. 1996, *ApJ*, 464, 985
- Birn, J., Forbes, T. G., & Hesse, M. 2006, *ApJ*, 645, 732
- Carmichael, H. 1964, in *The Physics of Solar Flares*, ed. W. N. Hess, 451
- Cliver, E. W., Dennis, B. R., Kiplinger, A. L., Kane, S. R., Neidig, D. F., Sheeley, Jr., N. R., & Koomen, M. J. 1986, *ApJ*, 305, 920

- Dulk, G. A. & McLean, D. J. 1978, *Sol. Phys.*, 57, 279
- Fan, Y. 2005, *ApJ*, 630, 543
- Fan, Y. & Gibson, S. E. 2007, *ApJ*, 668, 1232
- Frost, K. J. & Dennis, B. R. 1971, *ApJ*, 165, 655
- Gibson, S. E. & Fan, Y. 2006, *ApJ*, 637, L65
- Gilbert, H. R., Alexander, D., & Liu, R. 2007, *Sol. Phys.*, 245, 287
- Gilbert, H. R., Holzer, T. E., & Burkepile, J. T. 2001, *ApJ*, 549, 1221
- Gilbert, H. R., Holzer, T. E., Burkepile, J. T., & Hundhausen, A. J. 2000, *ApJ*, 537, 503
- Green, L. M., Kliem, B., Török, T., van Driel-Gesztelyi, L., & Attrill, G. D. R. 2007, *Sol. Phys.*, 246, 365
- Grigis, P. C. & Benz, A. O. 2008, *ApJ*, 683, 1180
- Hirayama, T. 1974, *Sol. Phys.*, 34, 323
- Hudson, H. S. 1978, *ApJ*, 224, 235
- . 2000, *ApJ*, 531, L75
- Kopp, R. A. & Pneuman, G. W. 1976, *Sol. Phys.*, 50, 85
- Krucker, S., Battaglia, M., Cargill, P. J., et al. 2008, *A&A Rev.*, 16, 155
- Krucker, S. & Lin, R. P. 2008, *ApJ*, 673, 1181
- Li, Y. P. & Gan, W. Q. 2007, *Advances in Space Research*, 39, 1389
- Lin, J. 2004, *Sol. Phys.*, 222, 115
- Lin, J., Soon, W., & Baliunas, S. L. 2003, *New Astron. Rev.*, 47, 53
- Liu, R., Alexander, D., & Gilbert, H. R. 2007, *ApJ*, 661, 1260
- Liu, R., Gilbert, H. R., Alexander, D., & Su, Y. 2008a, *ApJ*, 680, 1508
- Liu, R., Wang, H., & Alexander, D. 2009a, *ApJ*, 696, 121
- Liu, R., Xu, Y., & Wang, H. 2009b, *ArXiv e-prints* 0905.4309
- Liu, W., Petrosian, V., Dennis, B. R., & Jiang, Y. W. 2008b, *ApJ*, 676, 704
- Manchester, IV, W., Gombosi, T., DeZeeuw, D., & Fan, Y. 2004, *ApJ*, 610, 588

- Masuda, S., Kosugi, T., Hara, H., Tsuneta, S., & Ogawara, Y. 1994, *Nature*, 371, 495
- Metcalf, T. R. & Alexander, D. 1999, *ApJ*, 522, 1108
- Neupert, W. M. 1968, *ApJ*, 153, L59
- Pick, M., Démoulin, P., Krucker, S., Malandraki, O., & Maia, D. 2005, *ApJ*, 625, 1019
- Romano, P., Contarino, L., & Zuccarello, F. 2005, *A&A*, 433, 683
- Sato, J., Kosugi, T., & Makishima, K. 1999, *PASJ*, 51, 127
- Somov, B. V. 2006, *Plasma Astrophysics, Part I: Fundamentals and Practice* (Springer Science+Business Media, LLC)
- Somov, B. V. & Kosugi, T. 1997, *ApJ*, 485, 859
- Sturrock, P. A. 1966, *Nature*, 211, 695
- . 1991, *ApJ*, 380, 655
- Sturrock, P. A., Weber, M., Wheatland, M. S., & Wolfson, R. 2001, *ApJ*, 548, 492
- Sui, L. & Holman, G. D. 2003, *ApJ*, 596, L251
- Sui, L., Holman, G. D., & Dennis, B. R. 2004, *ApJ*, 612, 546
- Tomczak, M. 2001, *A&A*, 366, 294
- Tripathi, D., Gibson, S. E., Qiu, J., Fletcher, L., Liu, R., Gilbert, H., & Mason, H. E. 2009, *A&A*, 498, 295
- Veronig, A. M., Brown, J. C., Dennis, B. R., Schwartz, R. A., Sui, L., & Tolbert, A. K. 2005, *ApJ*, 621, 482
- Veronig, A. M., Karlický, M., Vršnak, B., et al. 2006, *A&A*, 446, 675
- Warmuth, A., Holman, G. D., Dennis, B. R., Mann, G., Aurass, H., & Milligan, R. O. 2009, *ApJ*, 699, 917